LAWRENCE
LIVERMORE
NATIONAL
LABORATORY

LLNL-JRNL-520611

Rendezvous Maneuvers of Small Spacecraft Using Differential Lift and Drag

M. Horsley, S. Nikolaev, A. Pertica

December 16, 2011

JOURNAL OF GUIDANCE, CONTROL, AND DYNAMICS

Disclaimer

Small Satellite Rendezvous Using Differential Lift and Drag

M. Horsley[1], S. Nikolaev[2], and A. Pertica[3]
Lawrence Livermore National Laboratory, Livermore, CA, 94550

The potential benefits of using small satellites are expected to increase if they are operated in groups to form 'virtual' satellites, which have the same functionality of a much larger satellite, but at a fraction of the cost. Unfortunately, due to third body gravitational forces, solar radiation pressure, and other perturbing forces, the satellites will drift apart if no control mechanism is employed to maintain the formation. This work describes a passive technique that uses the differential aerodynamic forces experienced by two spacecraft to exert a modest amount of control over their relative motion. Each spacecraft is assumed to possess a simple flat plate, which can be oriented to produce aerodynamic lift and drag. A control law is developed that allows the relative positions of the satellites to be controlled by adjusting the orientations of the plates. A simulation of a group of 2 small satellites will be performed to demonstrate the effectiveness of the method.

Nomenclature

A = surface area of flat plate

$a_{lift,\ drag}$ = magnitude of accelerations due to lift, drag

$C_{L,D}$ = coefficients of lift, drag

e = time varying eccentricity of harmonic oscillator motion

m = spacecraft mass

t = time

[1] Physicist, Physical and Life Sciences, Lawrence Livermore National Laboratory, 7000 East Avenue, Livermore, CA, Mail Stop L-210, horsley1@llnl.gov.
[2] Physicist, Physical and Life Sciences, Lawrence Livermore National Laboratory, 7000 East Avenue, Livermore, CA, Mail Stop L-210, nikolaev2@llnl.gov.
[3] Physicist, Physical and Life Sciences, Lawrence Livermore National Laboratory, 7000 East Avenue, Livermore, CA, Mail Stop L-210, pertica1@llnl.gov.

$u_{x,y,z}$ = control variables in x, y and z directions

$\vec{v}$ = velocity of spacecraft

$\hat{v}$ = spacecraft velocity unit vector

x,y,z = position coordinates of chaser in local-vertical/local-horizontal

$\hat{n}$ = normal vector of flat plate

γ, l = direction cosines

V_{inc} = velocity of the incident molecules

V_{re} = velocity of the reemitted molecules

R = universal gas constant

T_{inc} = temperature of the incident molecule

M_a = mean molecular mass of the atmosphere

T_a = temperature of the ambient atmosphere

s = molecular speed ratio

α_{accom} = accommodation coefficient

ω = target's circular orbit angular velocity

ρ = atmospheric density

$\bar{x}, \bar{y}$ = average position of chaser satellite

α, β = auxiliary variables describing difference between instantaneous and average position

$F_{10.7}$ = 10.7 cm solar radio flux index

A_p = geomagnetic activity index

I. Introduction

This paper describes a method for controlling the relative positions of a pair of small satellites using the differential aerodynamic forces experienced by the satellites in Low Earth Orbit (LEO). Small satellites are quickly

gaining in popularity for scientific [1-3], commercial [4, 5] and military applications [6], primarily due to the significant cost advantages when compared to larger satellites. Small satellites are inexpensive to produce and launch and are capable of performing many of the functions traditionally done by much larger satellites. A number of papers have advocated flying a group of small satellites in formation, which should make it possible to improve performance greatly (e.g. [7-9]). However, this requires the capability of assembling the group of satellites into a formation, and then maintaining the formation for the duration of the mission. In principle, on-orbit assembly and formation keeping can be performed using rocket engines. In the case of small satellites (e.g. CubeSats), this is proving to be difficult due to the challenge of designing propulsion systems that conform to the stringent mass, volume and power budgets characteristic of small satellites, see [10] for an excellent review. In addition, one of the cost saving advantages of small satellites is the possibility of ridesharing, i.e. taking advantage of the spare capacity available in a typical space launch. However, this usually requires the permission of the owners of the primary satellites being lifted into orbit. This permission is unlikely in cases where the small satellite introduces additional risk, such as is the case when a rocket engine is part of the small satellite's design.

Instead of relying on a rocket for propulsion, other forces can be used to provide control over the relative motion of the satellites. Techniques using aerodynamic drag and lift have been developed for performing aeroassisted orbital maneuvers such as aerobraking and performing plane changes, see [11, 12] for examples. These techniques typically rely on satellites with highly elliptical orbits which have perigees in the upper atmosphere. At these altitudes, the satellite's speed and atmospheric density are great enough to generate drag- and lift-induced accelerations that are sufficient for performing aerobraking / plane changes within a short period of time (i.e. a few orbital periods). In principle, these same forces can be used to perform maneuvers at higher altitudes, using satellites having circular orbits. In [13-15] techniques are studied to provide control over the relative motion of two or more satellites by taking advantage of the difference in drag experienced by the satellites. A serious drawback to using differential drag is that it only allows control over the relative motion in the orbital plane of the target spacecraft. Out-of-plane motion cannot be controlled using differential drag [13]. However, aerodynamic lift acts in a direction orthogonal to drag and offers the potential of controlling the motion in the out-of-plane direction. Thus, by combining the actions of differential drag and lift, it should be possible to perform formation flying maneuvers in all three translational degrees of freedom.

Generally, aerodynamic lift is much weaker than drag, which will limit its applicability to controlling the relative motion of a group of CubeSats to lower altitudes where the atmospheric density is sufficiently large. Practically, the relative accelerations induced by lift are small, and thus it is likely the most benefit will come from using lift and drag together to rendezvous or to maintain a formation of small satellites that are already close together. Using lift alone to perform on-orbit assembly is possible, though may be impractical due to relatively large maneuver distances and an excessive amount of time to complete the necessary maneuvers.

The paper is organized in the following manner. Section II will introduce aerodynamic force models appropriate for satellites in Low Earth Orbit (LEO) and discuss the effect of aerodynamic lift at these altitudes. Section III will discuss the equations of motion governing the relative motions of a pair of LEO satellites. A simple control law for controlling the relative position and velocities of two small satellites in all three dimensions using differential lift and drag is developed and demonstrated in section IV. Finally, the last section offers a short discussion on the merits of using differential lift to control the out-of-plane motion of a pair of small, LEO satellites flying in formation.

The main contribution of this paper is a description of a control algorithm that utilizes both aerodynamic lift and drag in order to control the relative spacing of two spacecraft in all three dimensions. This is significant because the only other viable option is to use a rocket engine, which is costly, reduces the available power and payload, and increases mission risk. We first reported the use of lift to control the motion in the out-of-plane direction in a previous work [16]. Here, we extend this method and demonstrate the use of lift and its benefits for controlling the relative in-plane and out-of-plane motions.

II. Aerodynamic Forces at Orbital Altitudes

In general, an object traveling through the Earth's atmosphere will experience aerodynamic forces that can be decomposed into two terms, drag and lift. Drag acts in the opposite direction of the velocity relative to the atmosphere, and lift acts in a direction which depends on the orientation of the spacecraft and is perpendicular to drag. In most cases involving LEO satellites, drag will tend to dominate (see [17], [18]). In fact, in most practical cases lift will be negligible. There are a number of reasons for this. First, satellites that are spinning/tumbling tend to have the effect of aerodynamic lift cancel out, yielding negligible effect on the orbit. Also, satellites with certain symmetrical shapes will tend to have the effect of the aerodynamic lift force cancel out. However, as pointed out in

[18], satellites that have stabilized attitudes may be subjected to a steady or periodic lift, leading to measurable effects on the orbit. By arranging for a large, flat stabilized surface (i.e. a plate) to be exposed to the atmosphere, it is possible to generate a small amount of lift acting on the satellite in a controllable fashion. For two LEO satellites in close proximity, it should be possible to control the relative acceleration in the out-of-plane direction by controlling the relative orientations of the plates. This approach differs from previous treatments of this problem, where the plates were arranged in such a way that only a differential drag force was generated [13-15].

There are a number of papers dealing with the effects of aerodynamic lift at orbital altitudes, see [18-20]. Nevertheless, lift at LEO altitudes is generally considered to be zero, or nearly zero, for the reasons given above. Because of this, a brief review of aerodynamic lift (and drag) at LEO altitudes will be given, followed by a detailed calculation of the lift (and drag) expected for a flat plate deployed by a small satellite.

The plate is assumed to be much larger than the body of the satellite, and hence any drag and lift caused by the satellite body will be neglected. For example, the plate could be a large solar array, or a structure created specifically for maneuvering purposes. The plate can be oriented in various ways by one or both satellites in order to generate a positive or negative relative acceleration. The aerodynamic drag and lift forces experienced by a flat plate can be represented by Eqs. (1a) and (1b)

$$F_{drag} = ma_{drag} = -\frac{1}{2}AC_D\rho|\vec{v}|^2 \tag{1a}$$

$$F_{lift} = ma_{lift} = -\frac{1}{2}AC_L\rho|\vec{v}|^2 \tag{1b}$$

where a_{drag} is the acceleration caused by the drag acting in the direction opposite of $\vec{v}$, a_{lift} is the acceleration caused by lift acting in the $(\hat{v}\times\hat{n})\times\hat{v}$ direction, $\hat{n}$ is the unit normal vector of the satellite plate, A is the total area of the plate, ρ is the atmospheric density, m is the mass of the satellite, $\vec{v}$ is the velocity of the satellite with respect to the atmosphere, and C_D and C_L are the coefficients of drag and lift, respectively. Here we are assuming $\vec{v}$ to be equal to the satellite's inertial velocity, and in effect we are neglecting the component of the atmospheric velocity that co-rotates with the earth. The coefficients of drag and lift are used to represent the effect of momentum transfer between the satellite and the surrounding atmosphere. The coefficients depend on the satellite shape and orientation, flow conditions and surface chemistry effects. Given the fact that lift at LEO altitudes is usually neglected, we will use a physics-based model in order to obtain a reasonable estimate of the lift and drag coefficients. At LEO altitudes

where the mean free path of a gas molecule is much larger than the size of the satellite, the coefficients of drag and lift can be computed exactly for cases involving simple shapes, like spheres, cylinders and flat plates. We will use the model described in [21] to compute the drag and lift coefficients, which is based on Sentman's treatment of lift and drag in free molecular flow conditions [22, 23] (with modifications due to Moe [24] in order to account for the effect of the accommodation coefficient, α_{accom}). The accommodation coefficient is a parameter that is used to capture some of the important aspects of the surface chemistry effects. In a sense, α_{accom}, describes how much memory the gas molecule retains of its initial velocity after its interaction with the satellite surface. Values of α_{accom} can vary from 0 to 1, and is approximately 0.9 at altitudes of 300 km [25]. Values of 1 indicate complete accommodation, meaning the emitted particle has a kinetic energy that has completely adjusted to the thermal energy of the surface. A number of papers review accommodation at orbital altitudes and the effects on satellites (see [24, 25] and references contained therein).

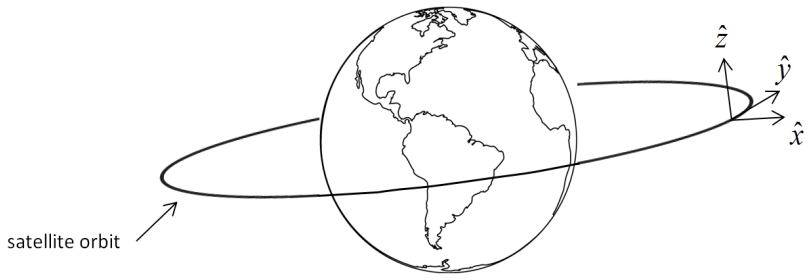

Figure 1. LVLH coordinate system.

At this point the Local Vertical Local Horizontal (LVLH) coordinate system will be introduced. We will assume the target satellite is moving in a circular orbit. The x axis points in the direction of the ray from the center of the Earth to the origin of the system (which moves in a circular orbit), the y axis is along the orbital track, and the z axis completes the right-hand Cartesian coordinate system. Following the treatment in [21], the coefficients of lift and drag for a one-sided flat plate in free molecular flow conditions are represented by Eqs. (2a) and (2b)

$$C_D = \frac{P}{\sqrt{\pi}} + \gamma Q Z + \frac{\gamma V_{re}}{2V_{inc}}\left(\gamma\sqrt{\pi}Z + P\right) \tag{2a}$$

$$C_L = lGZ + \frac{lV_{re}}{2V_{inc}}\left(\gamma\sqrt{\pi}Z + P\right) \tag{2b}$$

where $P = \dfrac{e^{-\gamma^2 s^2}}{s}$, $Q = 1 + \dfrac{1}{2s^2}$, $G = \dfrac{1}{2s^2}$, $Z = 1 + \mathrm{erf}(\gamma s)$, $\mathrm{erf}(x) = \dfrac{2}{\sqrt{\pi}}\int_0^x e^{-y^2}dy$.

In (2a) and (2b), γ refers to the cosine of the angle between $\hat{v}$ and the surface normal $\hat{n}$, while *l* refers to the cosine of the angle between $(\hat{v}\times\hat{n})\times\hat{v}$ and the surface normal, V_{inc} is the velocity of the incident molecules, V_{re} is the velocity of the reemitted molecules, R is the universal gas constant, T_{inc} is the temperature of the incident molecules $T_{inc} = V_{inc}^2/(3R)$, M_a is the mean molecular mass of the atmosphere, T_a is the temperature of the ambient atmosphere, s is the molecular speed ratio, $s = V_{inc}/\sqrt{2RT_a/M_a}$. In principle, contributions from the front and back sides of the plate should be taken into account when computing the coefficients of lift and drag. However, as pointed out in [26], for sufficiently high values of the speed ratio ($s \gtrsim 2$), the contribution from the back side is negligible. For LEO altitudes, this condition is satisfied and any contribution from the back side of the plate will be neglected for simplicity.

Using α_{accom}, the velocity of the re-emitted molecule relative to its incident velocity can be expressed as,

$$\frac{V_{re}}{V_{inc}} = \sqrt{\frac{2}{3}\left[1 + \alpha_{accom}\left(\frac{T_w}{T_{inc}} - 1\right)\right]} \tag{3}$$

where T_w is the surface temperature of the plate. The semi-empirical model described in [27] will be used to estimate the accommodation coefficient as input in Eq. (3). According to [27], the accommodation coefficient is related to the concentration of atomic oxygen at the altitude of the satellites, which is correlated with the Sun's effect on the Earth's atmosphere. The $F_{10.7}$ and A_p indices are typically used to characterize solar and geomagnetic activity (see [28] for an excellent review). The coefficients of lift and drag as a function of the angle of attack for a flat plate are computed using Eqs. (2a) and (2b), and shown in Fig. 2a, for an altitude of 350 km. The ratio of lift-to-drag at an angle of attack of 45 degrees is shown as a function of altitude in Fig. 2b. Based on the accommodation

model [27] and atmospheric parameters obtained from the NRLMSISE-00 model [29], the lift-to-drag ratio for a flat plate with a 45 degree angle of attack is predicted to vary from 0.09 – 0.17 at an altitude of 350 km. The ratio is predicted to increase as the altitude increases.

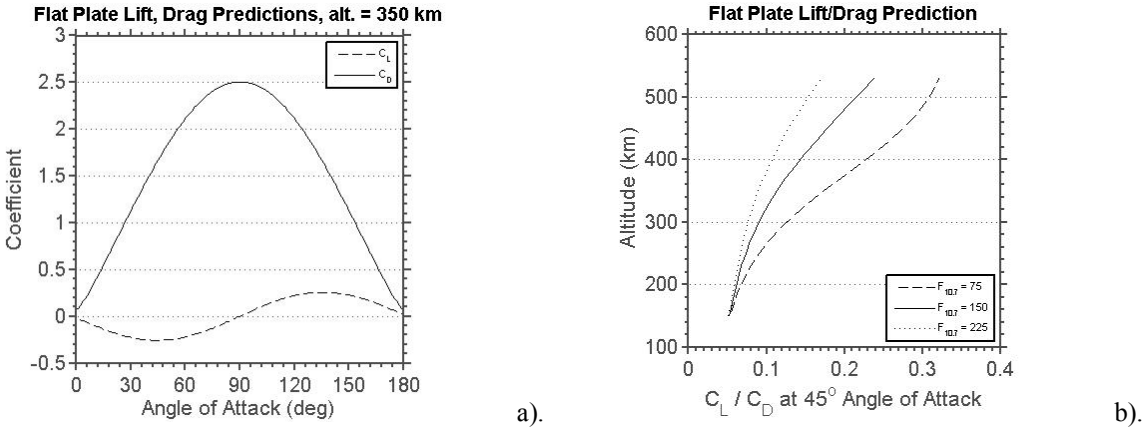

a). b).

Figure 2. (a) Flat plate predictions of lift and drag at 350 km, $F_{10.7}$ =150, A_p = 5. (b) The ratio of lift-to-drag for a fixed orientation is shown as a function of altitude for low, moderate and high levels of solar activity.

In order to generate differential accelerations between the target and chaser satellites, it will be necessary for the chaser satellite to arrange for its plate to have a certain orientation relative to the target satellite's plate. This can be done in a simple fashion by fixing a flat control plate to the satellite in a rigid manner and commanding the spacecraft to adopt an attitude such that the desired angle of attack of the plate with respect to the atmosphere is achieved. For simplicity, it will be assumed that the flat plate is square and is centered over the satellite's center of mass. For the idealized satellite discussed here, this configuration will not generate any net torques that would act to rotate the satellite. In practice, it can be expected that finite torques will be generated due to an imperfect manufacturing process used in constructing the small satellite. In order for the satellite to maintain the necessary angle of attack for the duration of the maneuver, we assume that any torques arising due to the imperfect construction will be compensated for by the satellite.

Thus, for this paper, we will assume that both satellites have an identical construction, and that each satellite is equipped with a large flat plate that can be positioned in one of 6 orientations and maintained in that orientation indefinitely (see Fig. 3). In order to generate a differential acceleration in the y direction, the target and chaser satellite will have to adopt similar lift and different drag profiles, as in Fig. 3, middle panel. In order to generate a

positive relative acceleration, the chaser satellite will maximize its drag while the target satellite will minimize its drag profile. Both satellites will maintain identical lift profiles. Generating a negative relative acceleration in the y direction is obtained when the target satellite maximizes its drag while the chaser satellite minimizes its drag profile. Changing the relative orientations of the two satellite's flat plates in this manner can be used to generate positive and negative accelerations in the y direction. No accelerations are generated in the x or z directions, because of the assumption of similar lift profiles.

In order to generate relative accelerations in the x direction, the satellites will have to adopt similar drag profiles, but different lift profiles. A simple approach is to require the two spacecraft to acquire similar angles of attack in the x-direction, but with opposite signs. For example, if it is desired to generate a positive relative acceleration in the x-direction, the chaser spacecraft will adopt an orientation as shown in the lower left panel of Fig. 3, where the outward pointing normal vector n_1 of its flat plate is $n_1 = [-0.707\ 0.707\ 0]$ and the outward normal vector n_2 of the target spacecraft is $n_2 = [0.707\ 0.707\ 0]$. Generating negative relative accelerations is accomplished by reversing the signs of the x-components of the two normal vectors. Relative accelerations in the z-direction can be obtained in a similar manner.

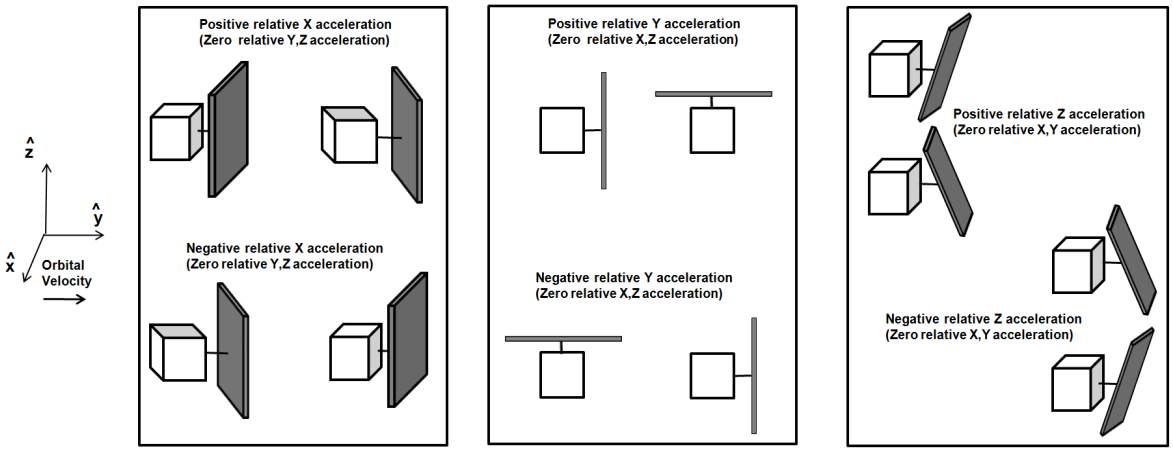

Figure 3. Relative orientations of spacecraft and resulting differential accelerations in the X, Y and Z directions. The middle panel was made with a slightly different orientation than the other panels, where the x axis is pointing straight out of the paper in order to better illustrate the orientation of the plate for each satellite.

III. Equations of Motion

The relative motion between two objects orbiting the Earth can be described in the classical LVLH coordinate system (see Fig. 1). In this coordinate system, the motion of the chaser satellite relative to the target satellite can be described using the Hill-Clohessy-Wiltshire equations:

$$\ddot{x} - 2\omega\dot{y} - 3\omega^2 x = u_x \tag{3a}$$

$$\ddot{y} + 2\omega\dot{x} = u_y \tag{3b}$$

$$\ddot{z} + \omega^2 z = u_z \tag{3c}$$

where ω is the orbital angular velocity of the target satellite, u_x, u_y, u_z are the relative accelerations due to the effect of lift and drag, and it is assumed the target satellite is in a circular orbit. The atmospheric density and accommodation coefficient will both be assumed to be constant for the duration of the maneuver. For simplicity, it will be assumed that when a differential acceleration, u, is applied that it will be in a single direction at a time, and that the possible values of the acceleration are fixed, u = a, 0, or $-a$. In the case where a differential acceleration is applied in the x direction, $u_y = u_z = 0$, and $u_x = -a_{lift}$, 0, or a_{lift}. The value of a can be computed from Eqs. (1) - (3). An example will be given for illustration. Assume the mass of the spacecraft is 10 kg, the area of the flat plate is 1 m^2, and at an altitude of 350 km each spacecraft will have a velocity of approximately 7.697 km/s. The mean atmospheric density at this altitude is 6.98×10^{-12} kg/m^3 [30]. Assuming $F_{10.7} = 150$, and $A_p = 5$, the magnitude of the coefficient of lift for a flat plate at an angle of attack of 45 degrees is $C_L \sim 0.25$. The acceleration experienced by a single spacecraft can be computed using Eq. (1). Since the orientations of two spacecraft are controlled such that their lift coefficients are equal in magnitude but opposite in sign, the differential acceleration is twice that computed using Eq. (1), yielding $a_{lift} \approx 1.03 \times 10^{-5}\ m/s^2$. The case where a differential acceleration is generated in the z direction can be handled in a similar manner, $u_y = u_x = 0$, and $u_z = -a_{lift}$, 0, or a_{lift}, and a_{lift} will have the same value as in the x case. When a differential acceleration is desired in the y direction, we have $u_x = u_z = 0$, and $u_y = -a_{drag}$, 0, or a_{drag}, and $a_{drag} \approx 5.15 \times 10^{-5}\ m/s^2$.

As is evident from Eq. (3), the motion in the x and y plane is coupled, and the motion in the z direction is independent of x or y. As described in section 2, differential accelerations can be generated by controlling the relative orientations of the flat plates attached to both spacecraft. The problem of controlling the motion in the x and y plane using only differential drag was first solved in [13]. Using differential drag alone results in differential accelerations in the y direction, which limits the effect of control to the x-y plane. We will now show how control can be extended to all three dimensions by exploiting the effect of differential lift as well as that of drag.

A. In-plane Motion

In order to demonstrate how control can be established, the approach used in [14] will be followed. The unforced solution can be described in the (x, y) plane and z-direction separately. In the (x, y) plane, the motion of the chaser relative to the target satellite will lie along a 2x1 ellipse. The average position of the chaser satellite will not change in the radial direction, but will drift in the along-track direction. The average position can be expressed as:

$$\bar{x} = 4x + 2\,\dot{y}/\omega \tag{4a}$$

$$\bar{y} = y - 2\,\dot{x}/\omega\,. \tag{4b}$$

In [13], an algorithm was described for controlling the location and size of the relative motion ellipse. Two auxiliary variables were introduced, α and β, to describe the difference between the instantaneous and average position variables

$$\alpha = -3x - 2\,\dot{y}/\omega = x - \bar{x} \tag{5a}$$

$$\beta = 2\,\dot{x}/\omega = y - \bar{y}\,. \tag{5b}$$

The eccentricity of the relative motion ellipse is given by $e = \sqrt{\alpha^2 + (\beta/2)^2}$, not to be confused with the orbital eccentricity.

In the case where control is exerted in the y-direction, $u_x = u_z = 0$, and $u_y = -a_{drag}$, 0, or a_{drag} and the transformation leads to a set of second-order, differential equations,

$$\ddot{\bar{y}} = -3a_{drag} \tag{6a}$$

$$\ddot{\beta} + \omega^2 \beta = 4a_{drag}. \tag{6b}$$

This transformation essentially reduces the relative motion to that of a double integrator, Eq. (6a), and a harmonic oscillator, Eq. (6b). The forced solutions can be solved analytically, see [13], and are:

$$\bar{x}(t) = \bar{x}_0 + 2\,a_{drag} t/\omega \tag{7a}$$

$$\bar{y}(t) = \bar{y}_0 - 3\omega\bar{x}_0\, t/2 - 3a_{drag}\, t^2/2 \tag{7b}$$

$$\alpha(t) = \alpha_0 \cos(\omega t) + \left(\frac{\beta_0}{2} - \frac{2a_{drag}}{\omega^2}\right)\sin(\omega t) \tag{7c}$$

$$\frac{\beta}{2}(t) = \left(\frac{\beta_0}{2} - \frac{2a_{drag}}{\omega^2}\right)\cos(\omega t) - \alpha_0 \sin(\omega t) + \frac{2a_{drag}}{\omega^2}. \tag{7d}$$

Eqs. (7a-d) describe the motion in the case where differential drag is used to control the formation. A similar set of equations can be derived for the case where differential lift is used, and the differential drag is zero. Here, the force is exerted in the x-direction, $u_y = u_z = 0$, and $u_x = -a_{lift}$, 0, or a_{lift} and the transformation leads to a set of second-order, differential equations:

$$\ddot{\bar{x}} = 0 \tag{8a}$$

$$\ddot{\alpha} + \omega^2 \alpha = a_{lift}\ . \tag{8b}$$

The forced solutions are

$$\bar{x}(t) = \bar{x}_0 \tag{9a}$$

$$\bar{y}(t) = \bar{y}_0 - 3\omega\bar{x}_0\, t/2 - 2\, a_{lift} t/\omega \tag{9b}$$

$$\alpha(t) = \left(\alpha_0 - \frac{a_{lift}}{\omega^2}\right)\cos(\omega t) + \frac{\beta_0}{2}\sin(\omega t) + \frac{a_{lift}}{\omega^2} \tag{9c}$$

$$\frac{\beta}{2}(t) = \frac{\beta_0}{2}\cos(\omega t) - \left(\alpha_0 - \frac{a_{lift}}{\omega^2}\right)\sin(\omega t). \tag{9d}$$

In the case where differential drag is used to effect control over the satellite formation, Eqs. (7a-b) describe the motion of the center of the ellipse. The motion is along one of a family of parabolas, as shown in Fig. (4a). Positive differential drag results in motion along one of the solid curves, and negative differential drag results in motion along one of the dashed parabolas. In cases where differential lift is used instead of drag, the state travels along a straight line parallel with the $\bar{y}$ axis. The rate will depend on the values of $\bar{x}_0$ and a_{lift}.

In the (α, β) plane, the motion is periodic. In Fig. (4b), α and $\beta/2$ are plotted for the case where differential drag is used (i.e. $u_x = u_z = 0$) for a variety of initial conditions. The motion is circular, with the centers located on the $\alpha = 0$ line and displaced along the β direction by an amount that depends on the value of a_{drag}. The radius arm has a magnitude e and rotates at an angular rate ω. In Fig. (4c), the motion is plotted for the case where differential lift is used (i.e. $u_y = u_z = 0$). While the motion is circular, as is the case with drag, there are a number of differences. First, the centers are located along the $\beta = 0$ line, and are displaced in the α direction by an amount that depends on the value of a_{lift}. Second, the magnitude of the displacement is reduced by a factor of 2 as compared to what is obtained in the case where drag is used to generate the differential accelerations. In all of these cases, no accelerations were present in the z direction, and hence the z motion corresponds to the unforced, oscillatory solution of Eq. (3c). The case where acceleration is present in the z direction will be discussed next.

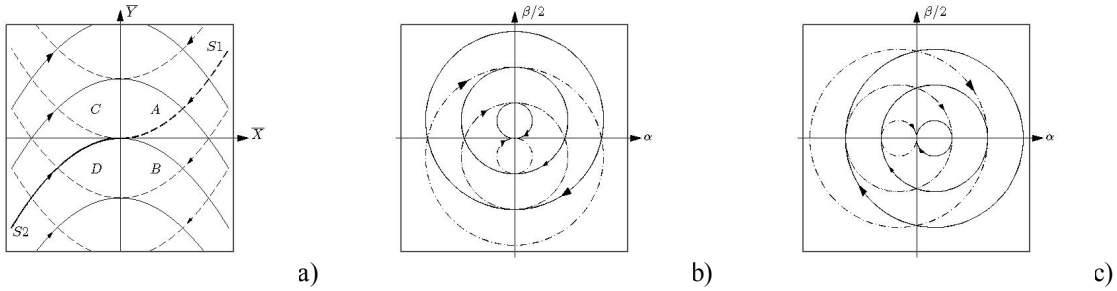

a) b) c)

Figure 4. Control trajectories in the (a) $\bar{x}$, $\bar{y}$ and (b, c) α, β planes. (a) and (b) corresponds to cases where differential drag is applied (no lift). (c) depicts the case where differential lift is applied (no drag). Positive (negative) accelerations indicated by solid (dashed) lines.

B. Out-of-Plane Motion

Positive and negative differential accelerations in the z direction are generated by controlling the relative orientations as shown in the right-most diagram in Fig. 3. The solution to Eq. (3c) can be shown by direct substitution to be

$$z(t) = \left(z_0 - \frac{a_{lift}}{\omega^2} \right) \cos(\omega t) + \frac{\dot{z}_0}{\omega} \sin(\omega t) + \frac{a_{lift}}{\omega^2} \tag{10}$$

where z_0 and $\dot{z}_0$ are the initial conditions, and a_{lift} can take on positive and negative values, as well as zero (i.e. coasting). The relative velocity, $\dot{z}$, is the time derivative of z . Scaling the relative velocity by $1/\omega$, the state moves along a circle in the $\left(z, \frac{\dot{z}}{\omega} \right)$ plane, see Fig. 5. The circles will be centered at $\left(\pm \frac{a_{lift}}{\omega^2}, 0 \right)$ for cases where a relative acceleration is present, or centered at the origin in cases where the two spacecraft are coasting.

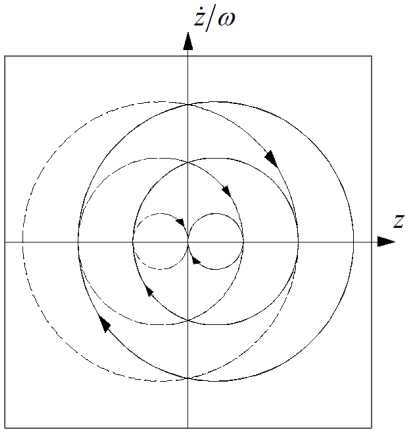

Figure 5. Control trajectories in the z, $\dot{z}/\omega$ plane. Positive (negative) accelerations indicated by solid (dashed) lines.

IV. Control

This section will describe how the analytical solutions developed in section 3 can be used in controlling the relative separation of two spacecraft in all three dimensions. Similar to the approaches described in [13] and [15], we will consider a control law consisting of a sequence of coasting, lift and/or drag accelerations. The strategy adopted here has two main parts. The first part, called the in-plane controller, deals with controlling the motion in the (x, y) plane. The second part, called the out-of-plane controller, deals with the motion in the z direction. Dealing separately with the in-plane and out-of-plane motions was done for the sake of simplicity, and was motivated by the decoupled nature of the motion. The in-plane controller shares similarities and differences with the orbit stabilization controller described in [13], where a two-phase maneuver was developed for rendezvous between two spacecraft using differential drag. The first phase, called the main control law, is designed to drive $\bar{x}$ and $\bar{y}$ to the origin while attempting to minimize the eccentricity. The second phase minimizes any remaining eccentricity. The in-plane controller developed in this paper is similar in the sense that it has two main parts designed to first drive $\bar{x}$ and $\bar{y}$ to the origin and then second, minimizes the eccentricity. However, what is new is the use of lift and drag in the control law used to minimize the eccentricity. Using lift and drag together can improve the performance when compared to the case where drag is used exclusively.

A. In-plane Controller – Phase 1

For simplicity, the first phase of the in-plane controller is identical to the main control law described in [14], where only drag is used to effect control over the relative position. Because of this, only a brief description will be given. The goal is to move the state towards one of the two switch curves, S1 or S2 in Fig. 4 a). If the initial state is in either the B or C quadrants, then the appropriate sign of the drag acceleration is chosen in order to move the state along a parabola towards the switch curve. The control is switched to ensure the sign of the differential drag acceleration has the same sign as α . This results in the eccentricity steadily decreasing as the maneuver develops. Because α moves in a harmonic fashion, this will occur exactly twice each orbit, and results in a distinctive saw tooth motion in the $(\bar{x}, \bar{y})$ plane. Once the state reaches the switch curve, the control that brings the state to the origin is exercised. Any remaining eccentricity will be eliminated in the second phase of the In-plane controller.

The phase 1 In-plane controller just described uses drag accelerations only. Augmenting drag-only control in $(\bar{x}, \bar{y})$-plane with lift-based maneuvers can help reduce the total maneuver time, by using horizontal trajectory segment to arrive to the switching curve sooner. Schematically, this case is similar to moving along the base of an isosceles triangle instead of following the trajectory along the sides. Due to the smallness of the lift acceleration, the improvement is modest, at the level of a few percent. In addition, lift+drag maneuvering is more efficient than pure drag for the small offsets from the origin in $(\bar{x}, \bar{y})$-plane, which makes lift maneuvers particularly suitable for e.g. formation flying.

B. In-plane Controller – Phase 2

In order to zero out the relative separation of the two spacecraft in the (α, β) plane, it will be necessary to execute a series of coasting, differential lift and/or drag maneuvers. However, this will affect the relative motion in the $(\bar{x}, \bar{y})$ plane. A sequence of maneuvers can be constructed that guarantees the relative separation in the $(\bar{x}, \bar{y})$ plane remains zero at the end of the Phase 2 maneuvers. There are a large number of maneuver sequences one can choose from that satisfy this requirement, with varying levels of complexity. In [15], a sequence of 4 maneuvers is constructed that zeroes out the relative separation in the (α, β) and $(\bar{x}, \bar{y})$ planes. Assuming the relative separation in the $(\bar{x}, \bar{y})$ has already been eliminated (as done in phase 1), the sequence consists of a coasting period

of t_w seconds, an application of differential drag for t_d seconds, followed by an application of differential drag of the opposite sign for $2t_d$ seconds, and then finishes with a period of differential drag applied for t_d seconds.

A new sequence of 3 differential lift maneuvers will now be described which zeroes out the relative separation in the (α, β) and $(\bar{x}, \bar{y})$ planes. When constructing this sequence of maneuvers, we will adopt the strategy described in [15], which starts at the origin, and propagating backwards in time, solves for the times required to arrive at the initial point. Based on Eqs. (9a) and (9b), it is clear that when starting at the origin, forced motion under differential lift in the $(\bar{x}, \bar{y})$ plane lies along the $\bar{y}$ axis, see Fig. 6a. The maneuver sequence starts with the application of a differential lift acceleration of arbitrary sign for t_1 seconds, reversing the acceleration and applying it for t_2 seconds, and then reversing the acceleration again and applying it for t_3 seconds. Determining the sign of the first differential lift acceleration (hence determining the remaining signs) will be described near the end of this section.

In order to guarantee $(\bar{x}, \bar{y})$ remains at the origin at the end of the maneuver sequence, it is sufficient that $t_2 = t_1 + t_3$. This differs from the drag-only case, Fig. 6b, where forced motion in the $(\bar{x}, \bar{y})$ plane lies along a parabola. In the drag-only case, the symmetry in the $(\bar{x}, \bar{y})$ plane requires the travel times for the first and third drag maneuvers to be identical, $t_1 = t_3 = t_d$, and the duration of the middle maneuver has to be twice that of the first (or third) maneuver, $t_2 = 2t_d$, in order to guarantee the relative separation in the $(\bar{x}, \bar{y})$ plane remains zero at the end of the sequence. Thus there is only a single free parameter, t_d, to use in the control. However, since both α and β have to be zeroed out, it will require in general two free parameters for control. The second control parameter can be obtained by introducing a coast period lasting for t_w seconds. In order to maintain the relative separation in the $(\bar{x}, \bar{y})$ plane to be at the origin, the coast phase is executed before the sequence of drag maneuvers occurs.

When considering a sequence of three differential lift maneuvers, the symmetry constraint is much weaker, and only requires that the duration of the second maneuver is equal to the sum of the first and last maneuvers, $t_2 = t_1 + t_3$, see Fig.6a. No coasting period is required, which is a significant advantage. Instead of having to wait a period of time t_w before initializing the sequence of differential drag maneuvers, control can be executed immediately using differential lift. The equations used to determine the control times t_1 and t_3 are derived in the following fashion. Starting at the origin, Eqs. (9c) and (9d) are used to compute the location after $-t_3$ seconds. The results of this

calculation are then used as the initial conditions, the sign of the acceleration is reversed and Eqs. (9c) and (9d) are again used to compute the location after $-t_2 = -(t_1 + t_3)$ seconds. Finally, the sign of the acceleration is reversed for the last time and the location is computed based on a period of $-t_1$ seconds, using the results of the previous calculations as the starting conditions. The equations corresponding to the computed α and β are set equal to the $\alpha^{phase\,1}$ and β^{phase1} achieved at the end of the Phase 1, and after some manipulations yields

$$0 = 2sin(\omega t_1 + 2\omega t_3) - sin(2\omega t_1 + 2\omega t_3) - 2sin(\omega t_3) - \frac{\beta^{phase1}}{2a_{lift}/\omega^2} \tag{11}$$

$$0 = 2cos(\omega t_1 + 2\omega t_3) - cos(2\omega t_1 + 2\omega t_3) - 2cos(\omega t_3) + 1 - \frac{\alpha^{phase1}}{a_{lift}/\omega^2}. \tag{12}$$

The Eqs. (11) and (12) must be solved numerically for t_1 and t_3, subject to the constraints $t_1 \in [0, 2\pi/\omega]$, $t_3 \in [0, 2\pi/\omega]$. The sign of the initial acceleration is determined by solving t_1 and t_3 for both sequences of maneuvers (+/-/+ and -/+/-) and selecting the maneuver sequence which yields the minimum total maneuver time.

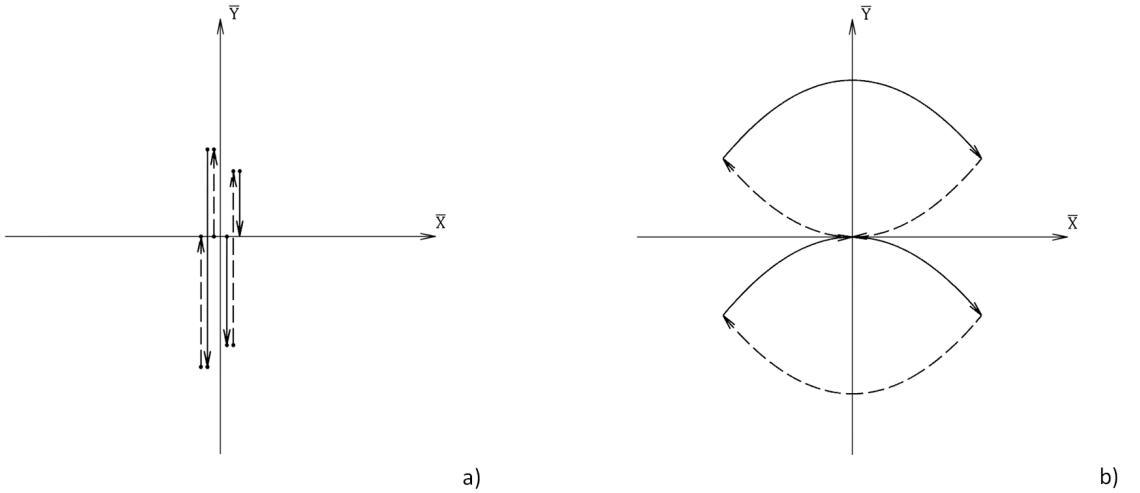

Figure 6. Control trajectories for phase 2 in-plane controller in the $(\bar{x}, \bar{y})$ plane. (a) Differential lift-based maneuvers for two different sequences. The left hand side of the plot shows the (-/+/-) sequence, and the right hand side of the plot shows the opposite case, (trajectories are slightly offset along X-axis for clarity); (b) Differential drag-based maneuvers for two different sequences. The top part of the plot shows the (-/+/-) sequence, and the bottom portion of the plot shows the opposite case. For a) and b), solid lines indicate positive acceleration, and the dashed lines indicate negative acceleration.

C. Out-of-plane Controller

A simple control algorithm will be presented that can be used to zero out the relative position and velocity between two small spacecraft in the z dimension. Since the out-of-plane motion is decoupled from the in-plane motion, no special precautions will have to be taken to ensure the solution obtained in the $(\bar{x}, \bar{y})$ and (α, β) planes remain unperturbed for the duration of the out-of-plane maneuver.

Imagine a point in the upper left corner of Fig. 5 (negative relative position and positive relative velocity). If the relative velocity could be controlled to be zero, the point would be located at $(-\Delta z_0, 0)$. Next, the relative orientations of the two spacecraft would be commanded to generate a net negative acceleration in the z direction. In this case the motion would be along one of the dashed-line circles. This acceleration would be maintained for exactly ½ an orbital period, where once again the relative velocity would be zero. However, the point is now at $(\Delta z_0 - 2a_{lift}/\omega^2, 0)$, a little closer to the origin. The spacecraft are now commanded to reverse the relative acceleration, and thus will travel along one of the solid-line circles. After exactly ½ an orbital period, the point will be located at $(-\Delta z_0 + 4a_{lift}/\omega^2, 0)$. In a single orbital period, the relative separation between the two spacecraft will have shrunk by an amount $4a_{lift}/\omega^2$. This process is continued until the relative position and velocity between the spacecraft is zeroed out. For arbitrary cases, it will be necessary to command the spacecraft to a point where the relative velocity is zero and the relative separation is an integer multiple of $4a_{lift}/\omega^2$. This can be accomplished by constructing a maneuver sequence consisting of a coasting period followed by an application of differential lift in the z direction for a period of time T_2, and then reversing the acceleration for an identical amount of time. In order to handle arbitrary cases, the following algorithm is presented.

Phase 3 Algorithm

Step 1: Coast for T_1 seconds

Step 2: Apply acceleration for T_2 seconds

Step 3: Reverse acceleration, apply for T_2 seconds

Step 4: Execute N times:

Reverse acceleration, apply for ½ orbital period

Reverse acceleration, apply for ½ orbital period.

The initial coast time, T_1, intermediate time T_2, and the number of iterations N can be found by starting at the origin and working backwards. In principle the sequence of signs for the accelerations should be chosen to minimize the total travel time. However, the total travel time is dominated by step 4, and so the initial sign of the acceleration was arbitrarily chosen to be positive. This makes the algorithm suboptimal, but only by a small amount. The number of iterations, N, is found by computing the integer that is equal to or less than the initial radius $R_0 = \sqrt{z_0^2 + \left(\dot{z}/\omega\right)^2}$, divided by the amount the relative separation decreases in a single orbital period, $N \le R_0 / \left(4 a_{lift} / \omega^2\right)$. After N iterations, the relative position and velocity will be $\left(z', 0\right)$, and the radius will be R'. Since the initial sign in the sequence of accelerations was arbitrarily chosen to be positive; this then determines the initial sign of the acceleration in step 2. The time T_2 is found by numerically solving for the time required to bring the radius R' to R_0, where T_2 is the travel time allowed for each section of the two part maneuver (steps 2 and 3 in the above algorithm). At this point in time, the relative position and velocity will be $\left(z'', \dot{z}''\right)$ which will be at the same radius as the initial starting point. The remaining step required is to coast for a time T_1, the value of which is found numerically.

D. Control Example

An example maneuver using the In-plane and Out-of-plane controllers described above will be given in this section. For this example, two small satellites will be controlled to rendezvous. The satellites will be modeled as described in section III, each having a mass of 10 kg and a 1 m^2 plate that can be oriented in one of 6 ways. For simplicity, we use $\omega = 0.001144$, and choose values for the lift and drag accelerations of $a_{drag} = 5 \times 10^{-5}\, m/s^2$ and $a_{lift} = 1 \times 10^{-5}\, m/s^2$, which are similar to the values predicted in section III. The initial conditions describing the separation in Cartesian coordinates (meters and meters/second) are summarized in table 1.

Table 1 Initial conditions for example.

Δx	Δy	Δz	$\Delta \dot{x}$	$\Delta \dot{y}$	$\Delta \dot{z}$
18.15	-678.16	31.07	-0.26	0.02	0.27

The relative separation of the two spacecraft is shown in Fig. 7 for Phase 1. The goal of Phase 1 is to zero out $\bar{x}$ and $\bar{y}$ (left panel Fig. 7). The maneuver starts at the point denoted with a square symbol, where a negative differential drag is applied (i.e. in the y direction) for 2723.38 seconds. At this point, denoted with a circle symbol, a positive differential drag is applied for 1482.39 seconds. At the end of this sequence of maneuvers, the separation in the $(\bar{x}, \bar{y})$ plane has been zeroed out. The Phase 1 maneuver, using differential drag only, required a total of 4205.77 seconds. The application of differential drag affected the relative motion in the (α, β) plane, (Fig. 7 middle panel) but had no influence on the motion in the out-of-plane direction, (Fig 7, right panel), where the motion was unforced.

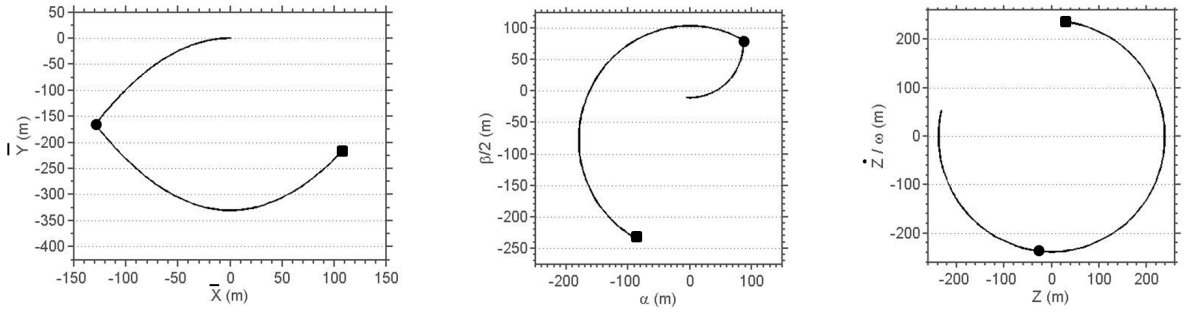

Figure 7 Relative separations of the two satellites during the Phase 1 maneuver. The initial conditions and values of the differential accelerations are given in the text. The square symbol marks the starting point of the maneuver, and the circle symbol marks the location where the sign of the differential drag acceleration was reversed.

The Phase 2 controller described above was then executed. This controller does not use differential drag, and instead relies on differential lift. The maneuver begins at the square symbol in Fig. 8 (left panel) by applying a positive differential lift (i.e. in the x direction) for 1094.09 seconds. The sign of the acceleration is reversed, (circle symbol in figure) and then held constant for 1592.51 seconds. Finally, the sign of the acceleration is reversed (star symbol in figure) and held steady for 498.42 seconds. This marks the end of the Phase 2 maneuver, where the relative

separation in the (α, β) plane has been eliminated. The Phase 2 maneuver, using differential lift only, required a total of 3185.02 seconds. Since $\bar{x}$ and $\bar{y}$ were zeroed out in Phase 1, the relative separation will remain zero since no differential drag was applied, as described in Eqs. (9a) and (9b). As in Phase 1, the motion in the out-of-plane direction was unforced.

The performance of the differential lift-only maneuvers for Phase 2 can be compared to the case where differential drag was used for control. Employing the same sequence of maneuvers as described in [15], the drag-only maneuver would require 5194.45 seconds, more than half of which is due to coasting. Thus, in this particular example the lift-only maneuver was completed in 60% of the time it would have taken using the drag-only maneuver. This is an example of the benefit of using differential lift for executing in-plane maneuvers. In some cases, the symmetric nature of the drag-only maneuvers requires an excessive coast period. Since the in-plane differential lift maneuver described above does not require a coast period, faster maneuver times can be obtained in some instances.

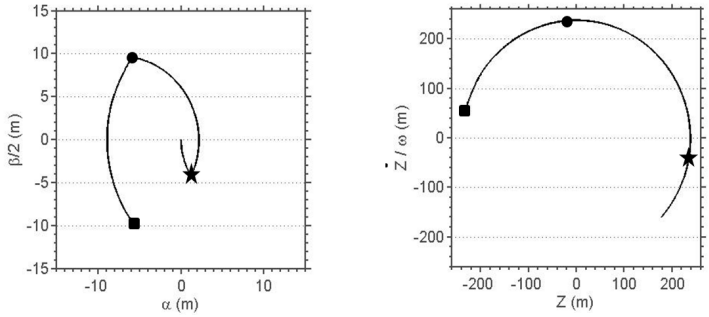

Figure 8. Relative separations of the two satellites during the Phase 2 maneuver. The square symbol marks the starting point of the maneuver, the circle symbol marks the location where the differential lift acceleration sign was switched, and the star symbol marks the point at which the sign of the differential lift acceleration was reversed for the last time.

Finally, once Phases 1 and 2 have been completed, the third and last phase can be executed, see Fig. 9. Using the Phase 3 control law described above, the relative position and velocity in the out-of-plane direction can be zeroed out. Taking z and $\dot{z}$ obtained after the completion of phase 2 as the initial conditions for phase 3, a coast period is executed for 1159.26 seconds. At this point, a negative differential lift acceleration is applied in the out-of-plane direction for 3247.71 seconds, which is then reversed and held constant for the same period of time. At this point the relative velocity in the out-of-plane direction is zero, and the step 4 from the Phase 3 algorithm is executed. This

particular example required 7 iterations. The total time required for the phase 3 maneuver is 26877.71 seconds, or 0.31 days.

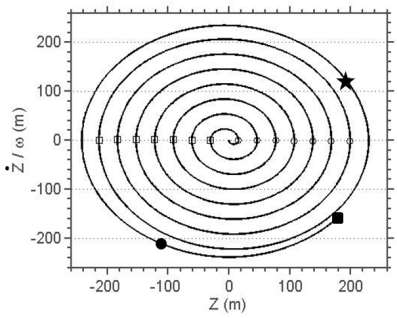

Figure 9. Maneuver sequence example for out-of-plane maneuver. The solid square symbol marks the starting point of the maneuver (i.e. step 1 in phase 3 algorithm). The solid circle symbol marks the beginning of step 2, and the star symbol marks the beginning of step 3. The end of the step 3 is marked with the left-most open square symbol, which coincides with the beginning of the iterative sequence (step 4). The open circle symbols indicate when the sign of the differential lift acceleration was changed from negative to positive, and the open square symbols indicate the opposite case.

V. Conclusion

Differential aerodynamic lift was introduced as a way to extend control over the in-plane and out-of-plane motions of a pair of small satellites. Used together with differential drag, this control technique allows the relative dynamics of two LEO satellites to be completely controlled using only aerodynamic forces. This is an important result because controlling the out-of-pane motion is not possible using differential drag, and would have required the use of a rocket engine. An important caveat in this work is the value of the coefficient of lift. In the past, the effect of aerodynamic lift on satellite orbits was assumed to be negligible and was ignored when considering formation flying maneuvers. Moreover, lift tends to cancel out for a variety of conditions related to the satellite's motion and geometry, making it difficult to find cases where the effect of lift is present. However, by maintaining a fixed orientation for extended periods of time, it is possible to have the effects of aerodynamic lift essentially build up over time and generate measurable effects on the satellite orbit. Section II discussed a physics-based approach for computing the coefficient of lift which indicates non-negligible lift at LEO altitudes, with lift-to-drag ratios of approximately 10-20% for a flat plate with an angle of attack of 45 degrees at 350 km, with increasing values at higher altitudes. While not as strong an affect as differential drag, differential lift in many cases offers modest

benefits for controlling the relative motion of two satellites in the plane of orbital motion. In particular, using aerodynamic lift is especially well-suited for small-scale maneuvering, e.g. formation keeping, due to the potential for continuous maneuvering (i.e. no coasting time). An additional benefit of using differential lift for performing these sorts of maneuvers is the reduction in the drag experienced by the satellites during the maneuver sequence. When executing a differential lift maneuver, the satellites are commanded to adopt similar drag but different lift profiles. Using the techniques outlined in section 2, this results in a reduction in the effect of drag by approximately 30 percent. This reduction in the effect of drag, coupled with the decrease in the maneuver time leads to a reduction in the altitude loss experienced by the satellites.

The authors wish to point out that the different nature of lift-only trajectories in $(\bar{x}, \bar{y})$ and (α, β) planes make lift-based maneuvering well-suited for complementing drag-based maneuvers. Instead of relying on a purely drag-based or lift-based maneuver sequence, a maneuver sequence composed of a combination of lift and drag based accelerations offers the potential of improving the performance over what can be achieved using either mode alone.

Finally, given the rather small number of studies on aerodynamic lift at orbital altitudes, a dedicated study of the effect would be beneficial and would help determine the utility of using lift for performing maneuvers. In particular, this method has great value for the studies of atmospheric effects on satellites. There has only been a very limited amount of satellite data that can be used to deduce accommodation coefficient, and only with poor time resolution (i.e. orbit- or daily-averages at best). Due to the sensitivity of C_L/C_D to accommodation, a satellite mission of this type has the potential to separate the effects of variations of accommodation from those of atmospheric density, making it possible to elucidate the effects of surface-atmosphere interactions. This has the potential to improve satellite tracking and orbit prediction models substantially.

Acknowledgments

This work was performed under the auspices of the U.S. Department of Energy by Lawrence Livermore National Laboratory under Contract DE-AC52-07NA27344. The Information Management release number for this document is LLNL-JRNL-520611. The authors wish to thank the anonymous reviewers for their many helpful comments and suggestions.

References

[1] Bahcivan, H., M. C. Kelley, and J. W. Cutler," Radar and rocket comparison of UHF radar scattering from auroral electrojet irregularities: Implications for a nanosatellite radar", *J. Geophys. Res*., 114, 2009, doi:10.1029/2009JA014132.

[2] Klumpar, D., Spence, H., Larsen, B., Blake, J., Springer, L., Crew, A., Mosleh, E., and Mashburn, K., "Spacecraft Thermal Control, Design, and Operation", *AIAA Guidance, Navigation, and Control Conference*, CP849, Vol. 1, AIAA, Washington, DC, 1989, pp. 103–115

[3] Crowley, G., Fish, C. S., Bust, G. S., Swenson, C., Barjatya, A., Larsen, M. F., "Dynamic Ionosphere Cubesat Experiment (DICE)". *American Geophysical Union, Fall Meeting 2009*.

[4] Greenland, S. and Clark, C., "CubeSat Platforms as an On-Orbit Technology Validation and Verification Vehicle", *Pestana Conference Centre* – Funchal, Madeira, Portugal*, 2010.*

[5] Helleren, Olsen, Narheim., "AISSat-1 - Demonstrating Operational Service from a Nano-Satellite", *Small Satellite Systems and Services Symposium (4S)*, Funchal, Madeira, Portugal, 2010.

[6] London, J. et al., "The First US Army Satellite in Fifty Years: SMDC-ONE First Flight Results", 2010 Small Satellite Conference, Logan, UT; Paper No. SSC11-III-5.

[7] Gill E., Runge H., "Tight Formation Flying for an Along-track SAR Interferometer", *Acta Astronautica* Vol. 55, No. 3-9, 2004. doi:10.1016/j.actaastro.2004.05.044

[8] Persson, S., Veldman, S., and Bodin, P., "PRISMA—A formation flying project in implementation phase", *Acta Astronautica,* Vol. 65, 2009, doi:10.1016/j.actaastro.2009.03.067

[9] D'Amico, S., Montenbruck, O., "Proximity Operations of Formation-Flying Spacecraft Using an Eccentricity / Inclination Vector Separation", *J. of Guid., Cont, and Dynamics*, Vol. 29, No. 3, May–June 2006

[10] Mueller, J., Marrese, C., Ziemer, J., Green, A., Yang, E., Mojarradi, M., Johnson, T., White, V., Bame, D., "JPL micro-thrust propulsion activities", 9 Sept. 2002. *AIAA Nanotech 2002,* Houston, TX

[11] El-Salam, F., "Optimization out-of-orbit plane changes using aeroassisted maneuvers", *Applied Math and Comp*., Vol. 170, No. 2 (2005). doi:10.1016/j.amc.2005.01.022

[12] Miele, A., "Recent Advance in the Optimization and Guidance of Aeroassisted Orbital Transfer". *Acta Astronautics*, 1996, 38(10): 747-768.

[13] Leonard, C., Hollister, W., Bergmann, E., "Orbital formation keeping with differential drag". *AIAA J. Guid. Control Dyn.* 12(1), 108–113 (1989)

[14] Bevilacqua, R., Hall, J., Romano, M., "Multiple Spacecraft Assembly Maneuvers By Differential Drag and Low Thrust Engines", *Celestial Mechanics and Dynamical Astronomy*, Vol. 106, No. 1 (2010) doi:10.1007/s10569-009-9240-3.

[15] Bevilacqua, R., Romano, M., "Rendezvous Maneuvers of multiple spacecraft using differential drag under J2 Perturbation". *AIAA J. Guid. Control Dyn*. 31(6), 2008

[16] Horsley, M., “An investigation into using differential drag for controlling a formation of CubeSats”, *AMOS Technical Conference*, Sept 13-16, 2011.

[17] Roy, A.E., Orbital Motion, Fourth Edition. Taylor & Francis (2005), pp. 337.

[18] Moore, P., “The effect of aerodynamic lift on near circular satellite orbits”, Planet. Space Sci., Vol 33, No. 5, 1985

[19] Harrison, Swinerd, ”Analysis of satellite laser ranging data to investigate satellite aerodynamics”, Planet. Space Sci, Vol. 43, No. 8 1995

[20] Harrison, Swinerd, “A free molecular aerodynamic investigation using multiple satellite analysis”, Planet. Space Sci., Vol. 44, No 2, pp 171-180. 1996

[21] Sutton, E., “Effects of Solar Disturbances on the Thermosphere Densities and Winds from CHAMP and GRACE satellite Accelerometer Data,” Ph.D. Dissertation, Aerospace Engineering Sciences, Univ. of Colorado, Boulder, , 2008.

[22] Sentman, L H, “Comparison of the Exact and Approximate Methods for Predicting Free Molecule Aerodynamic Coefficients,” *ARS Journal*, 1576-1579 (1961)

[23] Sentman, L H, “Effect of Degree of Thermal Accommodation on Free Molecule Aerodynamic Coefficients,” *ARS Journal*, 1408-1410 (1962a)

[24] Moe, K., Moe, M., Wallace, S., “Improved Satellite Drag Coefficient Calculations from Orbital Measurements of Energy Accommodation”, J*. of Spacecraft and Rockets*, Vol. 35, No. 3, 1998, pp. 266–272. DOI: 10.2514/2.3350

[25] Moe, K., Moe, M., “Gas-surface interactions and satellite drag coefficients”, Planetary and Space Science, Vol. 53, 2005, pp. 793–801. DOI: 10.1016/j/pss.2005.03.005

[26] Cercignani et al, “Free Molecular Flow Past a Flat Plate in the Presence of a Nontrivial Gas-Surface Interaction”, J. of Applied Mathematics and Physics, Vol. 23, 1972.

[27] Pilinski, M., Argrow, B., and Palo, S., “Semiempirical Model for satellite Energy-Accomodation Coefficinets”, *J. of Spacecraft and Rockets*, Vol. 47, No 6, 2010. DOI: 10.2514/1.49330

[28] Vallado, D., McClain, W., Fundamentals of Astrodynamics and Applications, New York, NY. McGraw-Hill (1997), pp. 521-532.

[29] J.M. Picone, A.E. Hedin, D.P. Drob, and A.C. Aikin, "NRL-MSISE-00 Empirical Model of the Atmosphere: Statistical Comparisons and Scientific Issues," *J. Geophys. Res.*, doi:10.1029/2002JA009430, (2003).

[30] Wertz and Larson (ed.), *Space Mission Analysis and Design*, 3rd ed, Space Technology Series, Microcosm Press, El Segundo, CA 1999, pp. 984.